

# The chain sucker: Translocation dynamics of a polymer chain into a long narrow channel driven by longitudinal flow

Kaifu Luo<sup>1,a)</sup> and Ralf Metzler<sup>2,3,b)</sup><sup>1</sup>CAS Key Laboratory of Soft Matter Chemistry, Department of Polymer Science and Engineering, University of Science and Technology of China, Hefei, Anhui Province 230026, People's Republic of China<sup>2</sup>Physics Department, Technical University of Munich, 85747 Garching, Germany<sup>3</sup>Physics Department, Tampere University of Technology, FI-33101 Tampere, Finland

(Received 15 February 2011; accepted 16 March 2011; published online 5 April 2011)

Using analytical techniques and Langevin dynamics simulations, we investigate the dynamics of polymer translocation into a narrow channel of width  $R$  embedded in two dimensions, driven by a force proportional to the number of monomers in the channel. Such a setup mimics typical experimental situations in nano/microfluidics. During the translocation process if the monomers in the channel can sufficiently quickly assume steady state motion, we observe the scaling  $\tau \sim N/F$  of the translocation time  $\tau$  with the driving force  $F$  per bead and the number  $N$  of monomers per chain. With smaller channel width  $R$ , steady state motion cannot be achieved, effecting a nonuniversal dependence of  $\tau$  on  $N$  and  $F$ . From the simulations we also deduce the waiting time distributions under various conditions for the single segment passage through the channel entrance. For different chain lengths but the same driving force, the curves of the waiting time as a function of the translocation coordinate  $s$  feature a maximum located at identical  $s_{\max}$ , while with increasing the driving force or the channel width the value of  $s_{\max}$  decreases. © 2011 American Institute of Physics. [doi:10.1063/1.3575239]

## I. INTRODUCTION

The transit of biopolymeric chains across membranes through nanopores, the *translocation* process, is a recurrent theme in cell biology.<sup>1–4</sup> In biological membranes the nanopore is typically constituted by a channel protein, the transmembrane proteins of the haemolysin family being a prominent example.<sup>5</sup> One family member,  $\alpha$ -haemolysin, is also often employed in single nanopore setups *in vitro*.<sup>6</sup> More recently, solid state nanopores in artificial supports, such as silicon compound membranes are manufactured by ion or electron beam techniques and open up the possibility for controlled technological applications.<sup>7,8</sup>

In biology, important examples for translocation processes are the passage of RNA or proteins through pores in the nuclear membrane, of proteins across mitochondrial and chloroplast membranes or through the endoplasmic reticulum, the cell-to-cell exchange of DNA across the cell walls, or the viral injection of RNA and DNA molecules.<sup>1</sup> In technology, biopolymer translocation is envisaged to be useful for rapid DNA sequencing, gene therapy, and, ultimately, toward controlled drug delivery.

The transport of biopolymers through a nanopore has attracted broad interest in the statistical physics community, as it represents a challenging problem in polymer physics.<sup>9–25</sup> A quantity of particular interest is the average translocation time  $\tau$  as a function of the chain length  $N$ , usually assumed to follow a scaling law  $\tau \sim N^\alpha$ . The scaling exponent  $\alpha$  hereby reflects the efficiency of the translocation

process. Thus, for completely directed (ratcheted) motion, one would expect  $\tau \sim N$ , while for normally diffusive unbiased translocation  $\tau \sim N^2$ .<sup>9,10</sup> Generally, the value of  $\alpha$  differs from these limiting behaviors, as effected by the entropic degrees of freedom of the chain-to-be-translocated. In particular, when the translocation dynamics is governed by unbiased anomalous diffusion<sup>26</sup> of the form  $\langle s^2(t) \rangle \sim t^\beta$  ( $0 < \beta < 1$ ) in terms of the translocation coordinate  $s$ , the value of the scaling exponent  $\alpha = 2/\beta$  becomes larger than 2.<sup>16,27</sup>

During the passage of a long flexible chain through a nanopore, its two extremities cannot access the volume opposite the membrane, and the monomer(s) in the pore are more or less unable to move. This reduction of the accessible degrees of freedom of the polymer involves a considerable entropic barrier during the pore passage. While unbiased translocation has been argued to feature the same scaling exponent  $\alpha = 1 + 2\nu$  as the free diffusion of the polymer by its radius of gyration,<sup>12–14</sup> where the Flory exponent is  $\nu = 0.588$  in 3D and  $\nu_{2D} = 0.75$  in 2D,<sup>28–30</sup> the associated prefactor is much larger.<sup>12</sup> Thus efficient polymer translocation requires the presence of driving forces. Most experimental<sup>6–8</sup> and theoretical<sup>16–24,31</sup> studies focus on the driving force provided by an external applied electric field, which mainly falls off across the pore. In this case,  $\alpha$  depends on the translocation dynamics. For slow translocation, i.e., under low driving force and/or high friction,  $\alpha \approx 1 + \nu \approx 1.588$  in 3D,<sup>16,32</sup> while  $\alpha \approx 1.37$  in 3D<sup>32</sup> for fast translocation due to the highly deformed chain conformation on the *trans* side, reflecting a pronounced nonequilibrium situation. In addition, for translocation achieved by pulling one end of the polymer with a constant force,  $\alpha \approx 2.0$  was

<sup>a)</sup> Author to whom correspondence should be addressed. Electronic mail: kluo@ustc.edu.cn.

<sup>b)</sup> Electronic mail: metz@ph.tum.de.

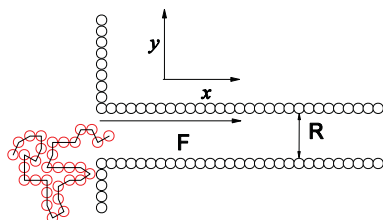


FIG. 1. Schematic representation of polymer translocation into a long 2D channel of width  $R$ . The driving force acting on the bead in the channel can be provided by an applied intrachannel electric field or a uniform flow of the solvent in the channel. We assume that the net force on the chain is proportional to the number of monomers,  $s(t)$ , in the chain.

established.<sup>16,33</sup> The above examples of translocation involve constant forces throughout the process. A different situation is encountered for translocating chains whose passage is effected by binding proteins, so-called chaperones or chaperonins.<sup>34</sup> Due to the fact that the chaperones bind more than one monomer of the chain-to-be-translocated, interesting variations occur in the effective driving force due to the “parking lot effect.”

Here we consider a case motivated by state-of-the-art fluidic nanochannel setups, in which the driving force grows constantly with the progress of the translocation process, until a saturation is reached when the entire chain is in the channel. In such setups one or multiple nanochannels branch off a micron-sized feeder channel (access hole).<sup>35,36</sup> The driving force is provided by the liquid flow: while the flow field is quite low in the feeder channel, the flow velocity is much higher inside the narrow channel. Once one end of the chain enters the nanochannel, it is veritably sucked inside, the overall drag force on the chain increases as more and more of the monomers enter the channel. Similarly, one might think of setups in which an electric field falls off in a long channel. If each monomer of the chain-to-be-translocated carries a net charge, the force acting on the chain will increase with the proportion of the chain inside the channel. This is not the case for the relatively short channel,<sup>37</sup> where the driving force cannot be proportional to the translocated monomers once the first monomer has passed through the pore. In many cases such fluidic setups are built in a pseudo-two-dimensional geometry, i.e., the channel is sandwiched between two parallel walls that are close to each other. Having such scenarios in mind we consider the geometry depicted in Fig. 1. We investigate this problem using analytical techniques and Langevin dynamics (LD) simulations. The paper is organized as follows. In Sec. II, we describe our model and the simulations technique. In Sec. III, we present and discuss our results. Finally, the conclusions are drawn in Sec. IV.

## II. MODEL AND METHODS

In our numerical simulations, the polymer chains are modeled as bead-spring chains of Lennard-Jones (LJ) particles with the finite extension nonlinear elastic (FENE) potential.<sup>38</sup> Excluded volume interactions between beads

are taken into consideration by a short range repulsive LJ potential:

$$U_{\text{LJ}}(r) = 4\epsilon \left[ \left( \frac{\sigma}{r} \right)^{12} - \left( \frac{\sigma}{r} \right)^6 \right] + \epsilon, \quad (1)$$

for  $r \leq 2^{1/6}\sigma$  and 0 for  $r > 2^{1/6}\sigma$ . Here,  $\sigma$  is the diameter of a bead and  $\epsilon$  is the potential depth. The connectivity between neighboring beads is modeled as a FENE spring with

$$U_{\text{FENE}}(r) = -\frac{1}{2}kR_0^2 \ln \left( 1 - \frac{r^2}{R_0^2} \right), \quad (2)$$

where  $r$  is the distance between consecutive beads,  $k$  is the spring constant, and  $R_0$  is the maximum allowed separation between connected beads.

We consider the geometry shown in Fig. 1: two strips with separation  $R$  consisting of stationary particles with a bead-bead distance  $\sigma$  form the walls of the channel, as well as the “membrane” containing the pore. Between all bead-wall particle pairs, there exists the same short range repulsive LJ interaction as described above. In the LD simulations, each bead is subjected to conservative, frictional, and random forces, respectively, with<sup>39</sup>

$$m\ddot{\mathbf{r}}_i = -\nabla(U_{\text{LJ}} + U_{\text{FENE}}) + \mathbf{F}_{\text{ext}} - \xi\mathbf{v}_i + \mathbf{F}_i^R, \quad (3)$$

where  $m$  is the bead mass,  $\xi$  is the friction coefficient for a single bead,  $\mathbf{v}_i = \dot{\mathbf{r}}_i$  is the bead velocity, and  $\mathbf{F}_i^R$  is the random force satisfying the fluctuation-dissipation theorem. The external force is expressed as  $\mathbf{F}_{\text{ext}} = F\hat{x}$ , where  $F$  is the external force strength per bead, exerted on the translocating beads located inside the channel, and  $\hat{x}$  is a unit vector in the direction along the channel. Therefore, the driving force for the whole chain is proportional to the number of translocated beads. Experimentally, this external driving force acting on the beads in the channel can be provided by an applied intrachannel electric field or a uniform flow of the solvent in the channel.

In the present work, we use the LJ parameters  $\epsilon$  and  $\sigma$  and the bead mass  $m$  to fix the energy, length, and mass scales, respectively. The time scale is then given by  $t_{\text{LJ}} = (m\sigma^2/\epsilon)^{1/2}$ . The dimensionless parameters in our simulations are  $R_0 = 2$ ,  $k = 7$ ,  $\xi = 0.7$ , and  $k_B T = 1.2$  unless otherwise stated. The Langevin equation is integrated in time by a method described by Ermak and Buckholz<sup>40</sup> in 2D.

Initially, the first bead of the chain is placed just inside the channel (at  $x = 0.75$ ,  $y = 0$ ), while the remaining beads are under thermal collisions described by the Langevin thermostat to obtain an equilibrium configuration. The translocation time is defined as the time duration between the beginning of the translocation and the last monomer entering into the channel. Note that, in contrast to many translocation setups, we allow the chain to escape from the channel back toward the *cis* side of the membrane. Typically, we average our data over 1000 independent runs.

Here, we should mention that the effect of hydrodynamic interactions is neglected in our simulation. Recent lattice Boltzmann<sup>41,42</sup> and molecular dynamics<sup>43</sup> simulation results show that hydrodynamics is screened out in a narrow pore, which is the case here and in the experiments.

### III. RESULTS AND DISCUSSION

In this section, we present our simulation results and discuss them in view of scaling arguments provided in the following subsection.

#### A. Scaling arguments

In standard translocation models, where the driving force acts solely in a short channel, only a single bead currently inside the channel experiences the driving force. For sufficiently slow translocation in the short nanopore, i.e., under low driving force and/or high friction, the exponent  $\alpha$  in the scaling law  $\tau \sim N^\alpha$  for the translocation time  $\tau$  can be estimated by the balance of driving force  $F$  and frictional force. The velocity of the center of mass along the direction of the driving force is  $v \sim F/\xi$ . The chain is not severely deformed during slow translocation processes, and the chain moves a distance of  $R_g$  during the translocation. Thus, the translocation time becomes  $\tau \approx R_g/v \sim N^{1+\nu} \xi/F$ .<sup>16,17,32</sup> Similarly, for polymer translocation under a constant pulling force acting on one chain end, the polymer travels a distance of  $R_{\parallel} \sim N$  during translocation, and  $\tau \approx R_{\parallel}/v \sim N^2 \xi/F$ .<sup>33</sup> However, if the external driving force is a function of time as for the present problem in a long channel with an intrachannel force, the translocation dynamics becomes different, as outlined in the following.

For a polymer of chain length  $N$  in a good bulk solvent in two dimensions (2D), the radius of gyration of the chain  $R_g$  scales as  $R_g \sim N^{\nu_{2D}} \sigma$ , where  $\nu_{2D} = 0.75$  is the Flory exponent in 2D and  $\sigma$  is the segment length. For a polymer confined between two strips embedded in 2D, the chain will extend along the channel to form blobs of size  $R$ , as long as  $R > \sigma$ . Each blob contains  $g \sim (R/\sigma)^{1/\nu_{2D}}$  beads, and the number of blobs is  $n_b = N/g \sim N(\sigma/R)^{1/\nu_{2D}}$ . The free energy cost for the chain confinement in units of  $k_B T$  is  $\mathcal{F} = N(\sigma/R)^{1/\nu_{2D}}$ .<sup>28</sup> The blob picture then predicts the longitudinal size of the chain to be  $R_{\parallel} = n_b R \sim N\sigma(\sigma/R)^{1/\nu_{2D}-1} \sim NR^{-1/3}$ .<sup>28</sup> The longitudinal relaxation time  $\tau_{\parallel}$  is defined as the time needed by a polymer to move a distance of the order of its longitudinal size,  $R_{\parallel}$ . Thus,  $\tau_{\parallel}$  scales as  $\tau_{\parallel} \sim R_{\parallel}^2/\tilde{D} \sim N^3 R^{-2/3}$ , where  $\tilde{D} \sim 1/N$  is the diffusion constant of the chain.

For a completely confined polymer in a 2D long channel under an external field, the total driving force is  $NF$  with  $F$  being the force acting on one bead. If the chain moves a distance of the order of  $R_{\parallel}$  under weak driving forces, the time cost can be estimated as  $\tau_{ss} \sim R_{\parallel}/v \sim NR^{-1/3}/F$ , where  $v \sim F$  is the velocity of the polymer. Under strong driving forces,  $R_{\parallel} \sim N$  is still correct,<sup>44</sup> but  $R_{\parallel} \sim R^{-1/3}$  breaks down due to the deformation of the blob and the elongation of the chain under the driving force. Thus, one can only obtain  $\tau_{ss} \sim N/F$ . For polymer translocation through a long channel with length  $L \gg R_g$ , we therefore obtain  $\tau_{ss} \sim L/v \sim 1/F$ , which is independent of  $N$ .<sup>45</sup> This steady state behavior in the channel, valid sufficiently far away from the two channel ends, is due to the fact that the force  $F$  acts uniformly on each monomer. The behavior is different when we consider the translocation time  $\tau$  measuring the time from threading

the first monomer into the channel until the moment when the entire chain is inside the channel.

To assess the capture of a polymer into the long channel under the influence of the intrachannel field, the situation is somewhat complicated due to the fact that the driving forces are proportional to the number of translocated beads. However, we still can give a rough estimate, if the chain monomers sufficiently quickly reach a steady state in the channel. If  $s(t)$  monomers are located inside the channel, the chain on the *cis* side experiences the friction force  $F_{cis,f}$  and the entropic force  $F_{cis,e}$ , while the translocating part experiences the friction force  $F_{trans,f}$ , the entropic force  $F_{trans,e}$ , and the driving force  $s(t)F$ . According to the balance of driving force, frictional forces, and entropic forces, we obtain the force relation:

$$F_{cis,f} + F_{cis,e} + F_{trans,f} + F_{trans,e} = s(t)F. \quad (4)$$

Based on the blob picture,

$$F_{trans,f} \approx \xi s(t) \frac{dR_{\parallel}(t)}{dt} \approx CR^{-1/3} \xi s(t) \frac{ds(t)}{dt} \quad (5)$$

with  $C$  being a constant. For a chain with size  $N = 128$  in a channel with  $R = 4.5$  in units of  $\sigma$ , the longitudinal size is  $R_{\parallel} \approx 90.73$ , and then we obtain  $C = 1.17$ . Once more than  $g$  monomers enter into the channel,  $F_{trans,e} \approx 2.12k_B T/R$  according to field-theoretical methods for 2D geometries (strips) and hard-wall boundaries.<sup>46</sup> Under the assumption that the chain on the *cis* side is close to its equilibrium state and is not severely deformed [ $F_{cis,e} R_g(N - s(t)) < k_B T$ ],  $F_{cis,e}$  can be estimated as  $F_{cis,e} \approx k_B T L_x / [R_g^2(N - s(t))]$ ,<sup>28</sup> with  $L_x$  being the elongation of the chain along the  $x$  direction. In addition,  $F_{cis,f} = \xi \sum_{i=s(t)+1}^N v_i$ , which under sufficiently slow translocation is negligible compared with  $F_{trans,f}$ , due to the much slower velocity. Thus, at the beginning of the translocation,  $F_{cis,e}$  plays an important role. However, once more than  $g$  monomers enter the nanopore,  $F_{cis,e}$  can be neglected compared with  $F_{trans,e}$ . Due to the fact that the driving force  $s(t)F$  increases over time, after reaching a critical  $s(t)$  the translocation dynamics is dominated by the balance between the driving force  $s(t)F$  and  $F_{trans,f}$ , particularly for larger  $F$  where  $F_{trans,e}$  becomes negligible. Then the translocation dynamics is dominated by

$$CR^{-1/3} \xi s(t) \frac{ds(t)}{dt} = s(t)F, \quad (6)$$

such that

$$\tau \sim \xi \frac{N}{F} R^{-1/3}. \quad (7)$$

If  $F_{trans,e}$  cannot be neglected, once more than  $g$  monomers enter into the channel, the translocation dynamics is controlled by

$$CR^{-1/3} \xi s(t) \frac{ds(t)}{dt} + F_{trans,e} = s(t)F, \quad (8)$$

such that

$$\tau \approx CR^{-1/3} \xi \frac{N}{F} - \frac{CR^{-1/3} \xi F_{trans,e}}{F^2} [1 - \ln(FN - F_{trans,e})]. \quad (9)$$

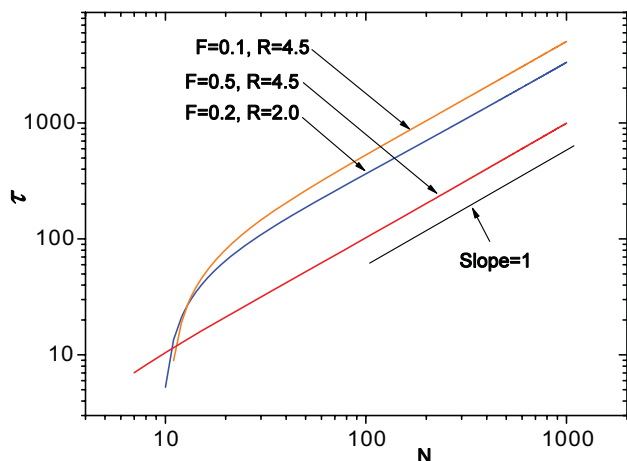


FIG. 2. Translocation time  $\tau$  predicted in Eq. (9) is plotted as function of chain length  $N$  for different channel widths  $R$  and driving forces  $F$ .

The results in Eqs. (7) and (9) are based on Eq. (5), where the equilibrium value of  $R_{\parallel}$  is used. As mentioned above, under strong driving forces  $R_{\parallel} \sim N$  is still correct, but  $R_{\parallel} \sim R^{-1/3}$  breaks down. Therefore, we do not expect the scaling exponents of  $\tau$  with  $R$  predicted in Eqs. (7) and (9) to be strictly correct. However, we can still use Eq. (9) with  $F_{trans,e} \approx 2.12 k_B T / R$  for the equilibrium state to estimate the scaling of  $\tau$  with  $N$ . Figure 2 demonstrates that the scaling  $\tau \sim N$  for long chains is fulfilled, and  $F_{trans,e}$  is thus important only for short chains.

If during the translocation process the monomers in the channel cannot sufficiently quickly assume steady state motion, the translocation dynamics is more complicated, as discussed in the following based on numerical results.

## B. Simulation results

We now proceed to present our numerical results and discuss them in the light of above scaling arguments.

### 1. Translocation probability as function of the driving force $F$ and channel width $R$

In our simulations initially the first monomer is held in place right at the channel entrance. After equilibration of the chain with fixed first monomer, the constraint is relieved. At high driving force  $F$ , already acting on the first monomer, the probability is relatively high that the chain will actually completely move into the channel, and not escape back to the *cis* side. At lower  $F$  retraction becomes more frequent. In this context we refer to a successful translocation as the event when the chain fully enters the pore, i.e., all  $N$  monomers are inside the channel such that the chain reaches the translocation coordinate  $s = N$ . If the first monomer retracts from the channel, the translocation is viewed as unsuccessful. In Fig. 3, we show the translocation probability of successful events as function of the driving force  $F$  and for different chain lengths  $N$ . For each value of  $F$  and  $N$  we perform as many translocation attempts until 1000 successful translocation events are reached. In the investigated force range the translocation probability increases almost linearly with the

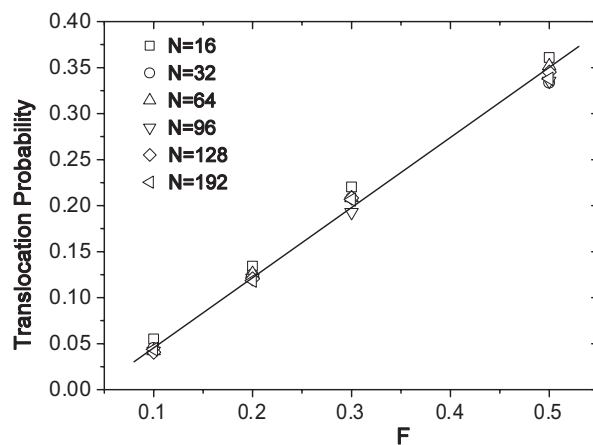


FIG. 3. Translocation probability as function of the driving force  $F$  for a fixed channel width  $R = 4.5$ . The results for various chain lengths approximately coincide. The line indicates a linear relation between the translocation probability and the driving force  $F$  per beads.

increasing translocation force  $F$ , and is approximately independent of the chain length  $N$ . This implies that it is important to capture the first few monomers in the channel, such that the overall force  $s(t)F$  reaches a sufficiently large value to prevent chain retraction from the pore.

Figure 4 depicts the translocation probability as function of the channel width  $R$  for two chain lengths, at driving forces  $F = 0.2$  and  $0.5$ . The resulting curves show an increase from quite small channel width toward wider channels, as expected. This is due to the decreased entropic resistance against threading of the chain into the channel. The approximate independence of the chain length suggests that this is, again, a more local effect: it matters to succeed sucking the first few monomers into the channel to ensure complete translocation. At larger values for  $R$  we observe a flattening of the curve, likely due to the elongation of the chain in the channel.

### 2. Translocation times as function of the chain length $N$ and channel width $R$

Figure 5 shows the translocation time  $\tau$  as function of the chain length  $N$  for different driving forces  $F$  and channel

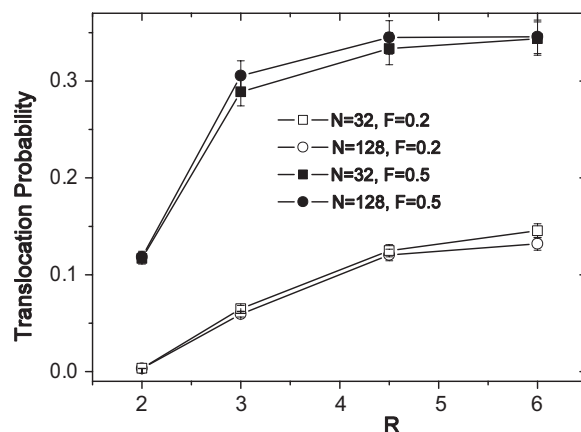


FIG. 4. Translocation probability as function of the channel width  $R$  for driving forces  $F = 0.2$  and  $0.5$ , and for two chain lengths.

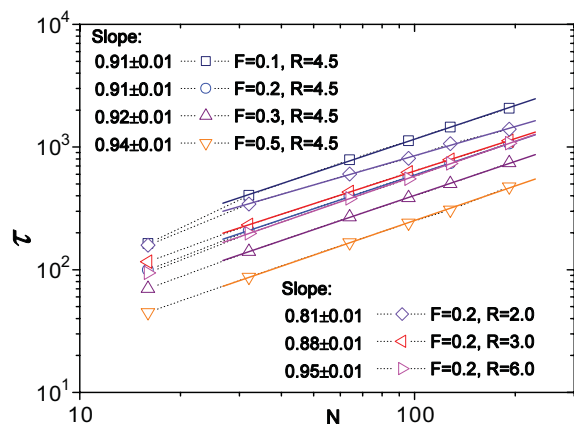


FIG. 5. Translocation time  $\tau$  as function of chain length  $N$  for different channel widths  $R$  and driving forces  $F$ .

widths  $R$ . For  $N \geq 32$ , a good scaling behavior  $\tau \sim N^\alpha$  is observed, with scaling exponent  $\alpha \approx 1$  for  $F = 0.1 \dots 0.5$  and  $R = 4.5$ , as well as for  $F = 0.5$  and  $R = 6.0$ . In these cases, the driving force dominates the translocation dynamics, and the value of  $\alpha$  is in agreement with the result (7) obtained from our scaling arguments. For  $N < 32$ ,  $F_{trans,e} \approx 2.12 k_B T/R$  increases and is no longer negligible for weak driving forces as predicted in Eq. (9) and plotted in Fig. 2. Decreasing  $R$  for fixed  $F = 0.2$ , the scaling exponent  $\alpha$  is reduced to  $0.88 \pm 0.01$ , and  $0.81 \pm 0.01$  for  $R = 3.0$  and  $2.0$ , respectively. The relaxation time of the chain increases with decreasing  $R$ , which leads to significant nonequilibrium situations. This factor leads to a more complicated translocation dynamics that can no longer be grasped by our simple scaling arguments leading to Eqs. (7) and (9). The resulting behavior, however, is good news: increasing the overall force exerted on the chain during the process of threading the chain into the channel leads to a more efficient translocation, with a scaling exponent smaller than one. It should be noted that once the entire chain is fully in the channel and reaches a steady state, the typical time to cover a distance  $R_{||}$  becomes independent of  $N$ , as shown above.

The radius of gyration of the polymer along the channel axis  $x$ , which is proportional to  $R_{||}$ , at the moment just after complete entrance into the channel, for different values of the

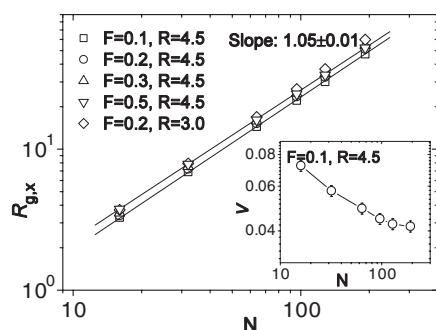


FIG. 6. Radius of gyration of the translocating polymer at the moment just after translocation, i.e., full entrance into the channel, for different translocation forces  $F$  and channel widths  $R$ . The inset shows the translocation velocity  $v$  as a function of the chain length  $N$ .

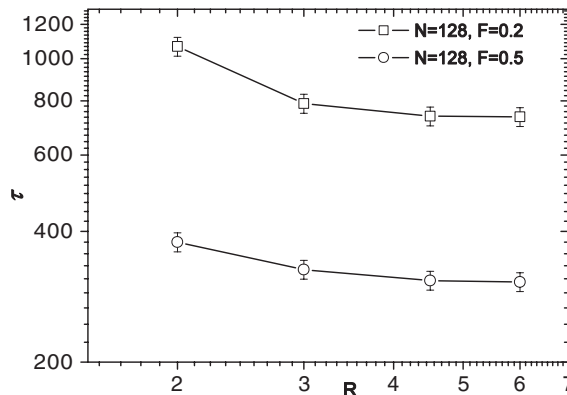


FIG. 7. Translocation time  $\tau$  as function of the channel width  $R$  for  $N = 128$  and  $F = 0.2$  and  $0.5$ .

translocation force  $F$  and channel width  $R$  turns out to follow the almost linear relation  $R_{g,x} \sim N$ . This is demonstrated in Fig. 6. This is perfectly in line with our scaling arguments for  $R_{||}$  developed above. The inset in Fig. 6 shows the translocation velocity, which decreases with the chain length  $N$ , and almost saturates for larger  $N$ . With the increasing channel width  $R$ , the translocation time decreases rapidly and then saturates for larger  $R$ , as shown in Fig. 7. Likely, this behavior is due to the decaying influence of the entropic force in the channel,  $F_{trans,e} \sim k_B T/R$  and the elongation of the chain under the driving force.

### 3. Translocation time as function of the driving force $F$

Figure 8 shows the translocation time  $\tau$  as function of the driving force  $F$  for different chain lengths  $N$ . We observe a behavior close to the predicted inverse proportionality with  $F$ ,  $\tau \sim F^{-1}$  from Eq. (5), for different chain lengths when the channel entropic force  $F_{trans,e} \sim k_B T/R$  is less pronounced. However, for smaller  $R$ , such as  $R = 2.0$ , the entropic force  $F_{trans,e}$  plays a more important role in the translocation dynamics: thus, for  $N = 64$  and  $R = 2.0$ , the chain cannot fully enter the nanopore at all, while for  $F \geq 0.2$ , we observe  $\tau \sim F^{-1.15}$ .

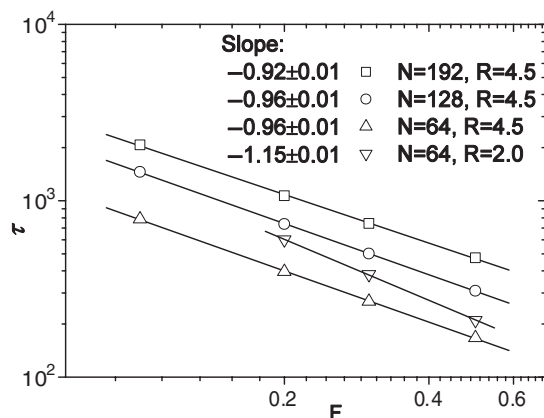


FIG. 8. Translocation time  $\tau$  as function of the driving force  $F$ .

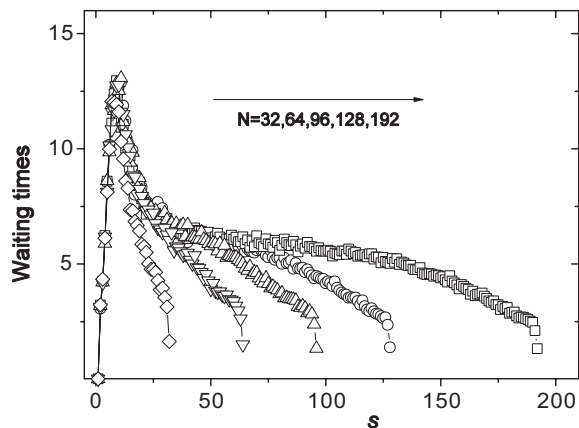


FIG. 9. Waiting time distribution for different chain lengths under driving force  $F = 0.2$  and with channel width  $R = 4.5$ . We define the waiting time of bead  $s$  as the average time between the events that bead  $s$  and bead  $s + 1$  move away from the channel entrance.

#### 4. Waiting time distribution

The dynamics of a single segment passing through the pore during translocation is an important quantity considerably affected by different driving mechanisms. The nonequilibrium nature of the translocation process has significant effects on this quantity. We numerically calculated the waiting times for all beads in a chain of length  $N$ . The waiting time of bead  $s$  for successful translocation hereby is defined as the average time between the events that bead  $s$  and bead  $s + 1$  move away from the channel entrance and further into the channel.

Figure 9 shows the waiting time distribution for different chain lengths under driving force  $F = 2.0$  and with channel width  $R = 4.5$ . Interestingly, the maximum waiting time occurs at  $s_{\max} \approx 10$  for all measured chain lengths. With increasing  $s$ , the waiting time increases rapidly to the maximum value, before a significantly softer decay. For increasing chain length a plateau appears. This form of the waiting time distribution again suggests that the initial capture of the chain in the channel is a local process, unaffected by the remainder of the chain on the *cis* side. At later stages of the process the leftover monomers are sucked into the channel more easily,

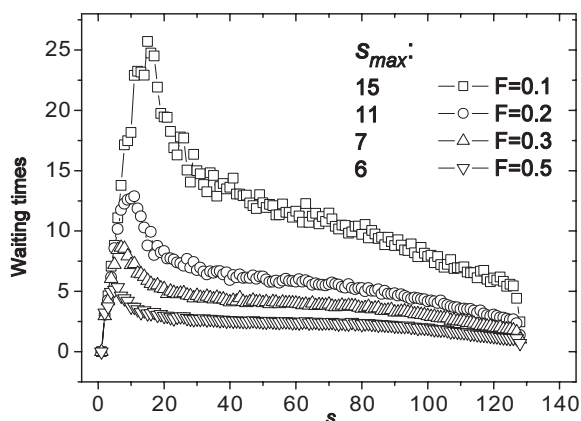


FIG. 10. Waiting time distribution under different driving forces for chain length  $N = 128$  and channel width  $R = 4.5$ .

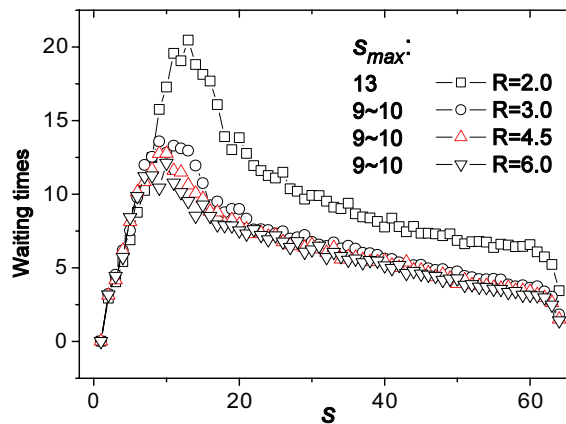


FIG. 11. Waiting time distribution for different channel width  $R$  and chain length  $N = 64$  under driving force  $F = 0.2$ .

due to the high force  $s(t)F$  reached by the  $s(t)$  monomers in the channel. Figure 10 shows the waiting time distribution under different driving forces  $F$ , for chain length  $N = 128$  and channel width  $R = 4.5$ . We observe that the number of monomers corresponding to the maximum waiting time,  $s_{\max}$ , shifts to smaller values with the increasing driving force, as one would expect. Increasing  $R$ , we find that  $s_{\max}$  rapidly decreases but saturates for larger  $R$ , compare Fig. 11.

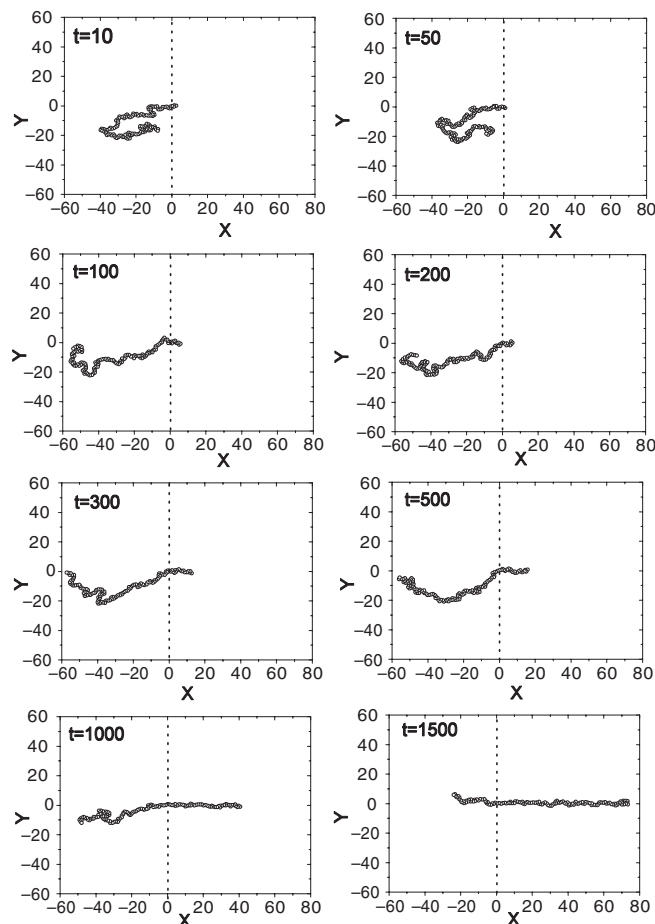


FIG. 12. Chain conformation during translocation for channel width  $R = 4.5$  and chain length  $N = 128$  under the driving force  $F = 0.1$ .

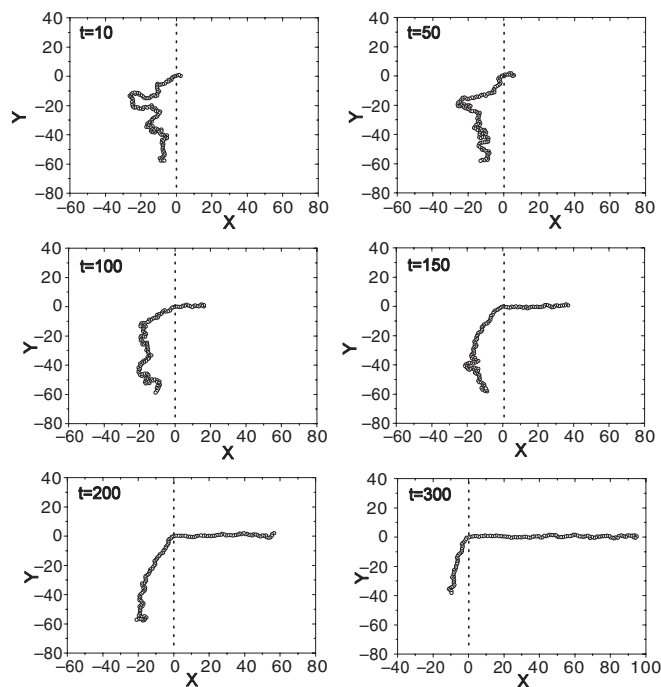


FIG. 13. Chain conformation during translocation for channel width  $R = 4.5$  and chain length  $N = 128$  under the driving force  $F = 0.5$ .

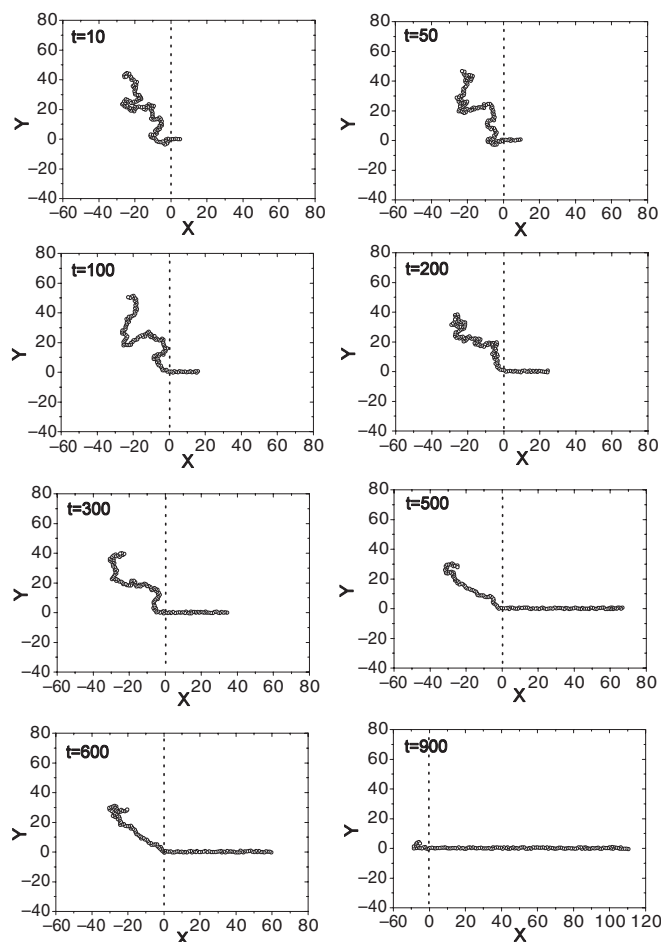


FIG. 14. Chain conformation during translocation for channel width  $R = 2.0$  and chain length  $N = 128$  under the driving force  $F = 0.2$ .

The coming into existence of nonequilibrium situations in the translocation process, we display typical chain configurations in the Appendix. Due to the increasing driving force  $s(t)F$ , the chain on the *cis* side experiences trumpet, stem-flower, and straight chain conformations during the translocation process, see Figs. 12–14.

#### IV. CONCLUSIONS

Using Langevin dynamics simulations, we investigated the dynamics of polymer translocation into a long channel embedded in a two-dimensional geometry, mimicking typical nano/microfluidic setups used, for instance, for DNA analysis. We analyzed how the translocation dynamics depends on the chain length  $N$  of the chain-to-be-translocated, the driving force  $F$ , and the channel width  $R$ . During the translocation process if the monomers in the channel can sufficiently quickly assume steady state motion, we observe the scaling  $\tau \sim N/F$  of the translocation time  $\tau$  with  $F$  and  $N$ . With smaller channel width  $R$ , steady state motion cannot be achieved, effecting a nonuniversal dependence of  $\tau$  on  $N$  and  $F$ . We also find that the waiting time distribution shows a maximum at the same translocation coordinate  $s_{\max}$  for different chain lengths, and  $s_{\max}$  decreases with the increasing driving force or channel width. We believe that this study opens up a new aspect to translocation studies, adding relevant quantitative information on the growing field of biopolymer analysis in nanochannels.

#### ACKNOWLEDGMENTS

K.L. acknowledges support from the University of Science and Technology of China through the Chinese Academy of Sciences (CAS) “Bairen” Program and the National Natural Science Foundation of China (Grant No. 21074126). R.M. acknowledges support from the Academy of Finland (FiDiPro scheme) and the Deutsche Forschungsgemeinschaft.

#### APPENDIX: TRANSLOCATION SNAPSHOTS

To get an idea of the translocation process, we show the typical chain conformation for different stages of the translocation process. The chain length  $N = 128$ . Figures 12 and 13 shows chain conformation during the translocation for channel width  $R = 4.5$  under the driving force  $F = 0.1$  and  $F = 0.5$ , respectively. For  $F = 0.1$ , at  $t = 100$  the typical trumpet chain conformation occurs. At  $t = 100$  and  $t = 1200$ , we observe the typical stem-flower conformation. Finally, the chain is almost straight at  $t = 1500$ . For  $F = 0.5$ , the chain is stretched to a straight conformation at  $t = 300$ . Figure 14 shows the chain conformation during translocation for channel width  $R = 2.0$  under the driving force  $F = 0.2$ . The chain in the channel is very straight during the translocation.

<sup>1</sup>B. Alberts, A. Johnson, J. Lewis, M. Raff, K. Roberts, and P. Walter, *Molecular Biology of the Cell* (Garland Publishing, New York, NY, 2002).

<sup>2</sup>A. Meller, *J. Phys.: Condens. Matter* **15**, R581 (2003).

<sup>3</sup>M. Muthukumar, *Annu. Rev. Biophys. Biomol. Struct.* **36**, 435 (2007).

- <sup>4</sup>T. A. Rapoport, *Nature (London)* **450**, 663 (2007).
- <sup>5</sup>See, for instance, B. B. Griffiths and O. McClain, *J. Basic Microbiol.* **28**, 427 (1988).
- <sup>6</sup>J. J. Kasianowicz, E. Brandin, D. Branton, and D. W. Deamer, *Proc. Natl. Acad. Sci. U.S.A.* **93**, 13770 (1996); M. Akeson, D. Branton, J. J. Kasianowicz, E. Brandin, and D. W. Deamer, *Biophys. J.* **77**, 3227 (1999); A. Meller, L. Nivon, E. Brandin, J. A. Golovchenko, and D. Branton, *Proc. Natl. Acad. Sci. U.S.A.* **97**, 1079 (2000); A. Meller, L. Nivon, and D. Branton, *Phys. Rev. Lett.* **86**, 3435 (2001).
- <sup>7</sup>M. Wanunu, J. Suntin, B. McNally, A. Chow, and A. Meller, *Biophys. J.* **95**, 1193 (2008); A. J. Storm, C. Storm, J. H. Chen, H. Zandbergen, J. F. Joanny, and C. Dekker, *Nano Lett.* **5**, 1193 (2005); U. F. Keyser, B. N. Koeleman, S. van Dorp, D. Krapf, R. M. M. Smeets, S. G. Lemay, N. H. Dekker, and C. Dekker, *Nat. Phys.* **2**, 473 (2006); C. Dekker, *Nat. Nanotechnol.* **2**, 209 (2007).
- <sup>8</sup>J. Li, D. Stein, C. McMullan, D. Branton, M. J. Aziz, and J. A. Golovchenko, *Nature (London)* **412**, 166 (2001); A. J. Storm, J. H. Chen, X. S. Ling, H. W. Zandbergen, and C. Dekker, *Nature Mater.* **2**, 537 (2003).
- <sup>9</sup>W. Sung and P. J. Park, *Phys. Rev. Lett.* **77**, 783 (1996).
- <sup>10</sup>M. Muthukumar, *J. Chem. Phys.* **111**, 10371 (1999).
- <sup>11</sup>M. Muthukumar, *J. Chem. Phys.* **118**, 5174 (2003).
- <sup>12</sup>J. Chuang, Y. Kantor, and M. Kardar, *Phys. Rev. E* **65**, 011802 (2001).
- <sup>13</sup>K. Luo, T. Ala-Nissila, and S. C. Ying, *J. Chem. Phys.* **124**, 034714 (2006).
- <sup>14</sup>K. F. Luo, S. T. T. Ollila, I. Huopaniemi, T. Ala-Nissila, P. Pomorski, M. Karttunen, S. C. Ying, and A. Bhattacharya, *Phys. Rev. E* **78**, 050901(R) (2008).
- <sup>15</sup>J. L. A. Dubbeldam, A. Milchev, V. G. Rostiashvili, and T. A. Vilgis, *Phys. Rev. E* **76**, 010801(R) (2007).
- <sup>16</sup>Y. Kantor and M. Kardar, *Phys. Rev. E* **69**, 021806 (2004).
- <sup>17</sup>K. F. Luo, I. Huopaniemi, T. Ala-Nissila, and S. C. Ying, *J. Chem. Phys.* **124**, 114704 (2006); *ibid.* **125**, 124901 (2006).
- <sup>18</sup>S. Matysiak, A. Montesi, M. Pasquali, A. B. Kolomeisky, and C. Clementi, *Phys. Rev. Lett.* **96**, 118103 (2006).
- <sup>19</sup>J. L. A. Dubbeldam, A. Milchev, V. G. Rostiashvili, and T. A. Vilgis, *Europhys. Lett.* **79**, 18002 (2007).
- <sup>20</sup>H. Vocks, D. Panja, G. T. Barkema, and R. C. Ball, *J. Phys.: Condens. Matter* **20**, 095224 (2008).
- <sup>21</sup>K. F. Luo, T. Ala-Nissila, S. C. Ying, and A. Bhattacharya, *J. Chem. Phys.* **126**, 145101 (2007); *J. Chem. Phys.* **99**, 148102 (2007); *ibid.* **100**, 058101 (2008); *Phys. Rev. E* **78**, 061911 (2008); *ibid.* **78**, 061918 (2008).
- <sup>22</sup>A. Bhattacharya, W. H. Morrison, K. Luo, T. Ala-Nissila, S. C. Ying, A. Milchev, and K. Binder, *Eur. Phys. J. E* **29**, 423 (2009); A. Bhattacharya and K. Binder, *Phys. Rev. E* **81**, 041804 (2010).
- <sup>23</sup>M. G. Gauthier and G. W. Slater, *J. Chem. Phys.* **128**, 205103 (2008).
- <sup>24</sup>T. Sakaue, *Phys. Rev. E* **76**, 021803 (2007); T. Sakaue, *ibid.* **81**, 041808 (2010).
- <sup>25</sup>A. Milchev, K. Binder, and A. Bhattacharya, *J. Chem. Phys.* **121**, 6042 (2004).
- <sup>26</sup>R. Metzler and J. Klafter, *Phys. Rep.* **339**, 1 (2000); *J. Phys. A* **37**, R161 (2004).
- <sup>27</sup>R. Metzler and J. Klafter, *Biophys. J.* **85**, 2776 (2003).
- <sup>28</sup>P. G. de Gennes, *Scaling Concepts in Polymer Physics* (Cornell University Press, Ithaca, NY, 1979); M. Daoud and P. G. de Gennes, *J. Phys. (Paris)* **38**, 85 (1977).
- <sup>29</sup>M. Doi and S. F. Edwards, *The Theory of Polymer Dynamics* (Clarendon, Oxford, 1986).
- <sup>30</sup>M. Rubinstein and R. Colby, *Polymer Physics* (Oxford University Press, Oxford, 2003).
- <sup>31</sup>S. T. T. Ollila, K. F. Luo, T. Ala-Nissila, and S. C. Ying, *Eur. Phys. J. E* **28**, 385 (2009).
- <sup>32</sup>K. Luo, T. Ala-Nissila, S. C. Ying, and R. Metzler, *EPL* **88**, 68006 (2009).
- <sup>33</sup>I. Huopaniemi, K. F. Luo, T. Ala-Nissila, and S. C. Ying, *Phys. Rev. E* **75**, 061912 (2007).
- <sup>34</sup>S. F. Simon, C. S. Peskin, and G. F. Oster, *Proc. Natl. Acad. Sci. U.S.A.* **89**, 3770 (1992); R. Zandi, D. Reguera, J. Rudnick, and W. M. Gelbart, *Proc. Natl. Acad. Sci. U.S.A.* **100**, 8649 (2003); T. Ambjornsson and R. Metzler, *Phys. Biol.* **1**, 77 (2004); T. Ambjornsson, M. A. Lomholt, and R. Metzler, *J. Phys. Cond. Matter* **17**, S3945 (2005); Y. Kafri, D. K. Lubelski, and D. R. Nelson, *Biophys. J.* **86**, 3373 (2004); R. Abdolvahab, M. R. Ejtehadi, and R. Metzler, *Phys. Rev. E* **83**, 011902 (2011).
- <sup>35</sup>J. O. Tegenfeldt, C. Prinz, H. Cao, R. L. Huang, R. H. Austin, S. Y. Chou, E. C. Cox, and J. C. Sturm, *Anal. Bioanal. Chem.* **378**, 1678 (2004).
- <sup>36</sup>L. H. Thamdrup, A. Klukowska, and A. Kristensen, *Nanotechnology* **19**, 125301 (2008).
- <sup>37</sup>T. Ambjornsson, S. P. Apell, Z. Konkoli, E. A. Di Marzio, and J. J. Kasianowicz, *J. Chem. Phys.* **117**, 4063 (2002).
- <sup>38</sup>K. Kremer and G. S. Grest, *J. Chem. Phys.* **92**, 5057 (1991).
- <sup>39</sup>M. P. Allen and D. J. Tildesley, *Computer Simulation of Liquids* (Oxford University Press, New York, 1987).
- <sup>40</sup>D. L. Ermak and H. Buckholz, *J. Comput. Phys.* **35**, 169 (1980).
- <sup>41</sup>A. Lzmitli, D. C. Schwartz, M. D. Graham, and J. J. de Pablo, *J. Chem. Phys.* **128**, 085102 (2008).
- <sup>42</sup>M. Fyta, S. Melchionna, S. Succi, and E. Kaxiras, *Phys. Rev. E* **78**, 036704 (2008).
- <sup>43</sup>M. G. Gauthier and G. W. Slater, *Eur. Phys. J. E* **25**, 17 (2008); S. Guillozic and G. W. Slater, *Phys. Lett. A* **359**, 261 (2006).
- <sup>44</sup>K. Luo and R. Metzler, *Phys. Rev. E* **82**, 021922 (2010).
- <sup>45</sup>H. S. Yong and K. F. Luo (unpublished).
- <sup>46</sup>T. W. Burkhardt and I. Guim, *Phys. Rev. E* **58**, 5833 (1999).